

Article

Mechanism for the Potential Inhibition Effect of Microcystin-LR Disinfectant By-Products on Protein Phosphatase 2A

Huiqun Yu, Yixue Xu, Jiyuan Cui and Wansong Zong *

College of Geography and Environment, Shandong Normal University, 88# East Wenhua Road, Jinan 250014, China

* Correspondence: 611029@sdsu.edu.cn; Tel./Fax: +86-531-89610039

Abstract: The secondary contamination of microcystin disinfection by-products (MC-DBPs) is of concern due to the residual structure similar to their original toxin. Based on identification and preparation, the potential inhibition effect of typical MCLR-DBPs (associated with the oxidation of Adda⁵) on PP2A was confirmed in the sequence of MCLR > P1 > P4 > P3 ≈ P2 > P7 ≈ P6 ≈ P5 > P8. To elucidate the molecular mechanism underlying the inhibition effect, the interaction models for typical MCLR-DBPs and PP2A were constructed using a modeling-based-on-ligand-similarity approach, and the candidate interaction parameters between typical MCLR-DBPs and PP2A were obtained by molecular docking. By analyzing the correlation between inhibition data and candidate interaction parameters, the key interaction parameters were filtered as hydrogen bonds "Adda⁵"←Asn₁₁₇, "Adda⁵"←His₁₁₈, MeAsp³←Arg₈₉, Arg⁴←Arg₂₁₄, Arg⁴→Pro₂₁₃; ionic bonds Glu⁶-Arg₈₉, Asp₈₅-Mn₁²⁺, Asp₅₇-Mn₂²⁺; and metal bonds Glu⁶-Mn₁²⁺, Glu⁶-Mn₂²⁺. With the gradual intensification of chlorination, Adda⁵ was destroyed to varying degrees. The key interactions changed correspondingly, resulting in the discrepant inhibition effects of typical MCLR-DBPs on PP2A.

Keywords: microcystin-LR; disinfection by-products; protein phosphatase 2A; molecular docking; molecular mechanism

Key Contribution: This manuscript established a feasible approach to evaluate the mechanism for the potential inhibition effect of typical MCLR-DBPs on PP2A at the molecular level.



Citation: Yu, H.; Xu, Y.; Cui, J.; Zong, W. Mechanism for the Potential Inhibition Effect of Microcystin-LR Disinfectant By-Products on Protein Phosphatase 2A. *Toxins* **2022**, *14*, 878. <https://doi.org/10.3390/toxins14120878>

Received: 9 September 2022

Accepted: 13 December 2022

Published: 16 December 2022

Publisher's Note: MDPI stays neutral with regard to jurisdictional claims in published maps and institutional affiliations.



Copyright: © 2022 by the authors. Licensee MDPI, Basel, Switzerland. This article is an open access article distributed under the terms and conditions of the Creative Commons Attribution (CC BY) license (<https://creativecommons.org/licenses/by/4.0/>).

1. Introduction

Microcystin (MC) pollution related to eutrophication has become a widespread concern of researchers around the world [1]. As the secondary metabolites from algal blooms, MCs are released into the water after algae cells die and rupture. MCs not only affect water quality, but also pose a serious threat to water ecosystems and public health and safety [2]. MCs are a class of cyclic heptapeptides that share the common structure cyclo-D-Ala¹-X²-D-isoAsp³-Z⁴-Adda⁵-D-isoGlu⁶-Mdha⁷ [3]. Due to variable amino acids at position X²/Z⁴ and methylation of other residues, more than 100 different MC isomers have been identified [4]. Among these MCs, MCLR is the most toxic and widespread isomer [5].

MCs have strong hepatotoxicity [6,7]. Acute poisoning is mainly manifested in liver redness, swelling and bleeding, destruction of the hepatocyte skeleton, and so on [8]. The toxic mechanism of MCs involves the inhibition of protein phosphatases (PPs, the main regulatory factors of protein dephosphorylation) [9]. Crystal structure analysis for MCLR-PPs complexes revealed that MCs undergo a two-step interaction with PPs [10,11]: in the first step, partial surface hydrophobic amino acid residues form a cage structure by hydrophobic interaction and quickly envelop the side chain of Adda⁵; in the second step, the C=C bond of Mdha⁷ is irreversibly bound to specific nucleophilic sites (typically cysteine residues) by electrophilic addition reaction. Finally, the important interactions

between the conserved domains of PPs (especially nine strictly conserved amino acids) and metal ions interacting with the introduced phosphate group change accordingly, resulting in the inhibition of PPs activity [12]. Consequently, the intracellular phosphorylated functional protein is overexpressed [13,14], resulting in massive hemorrhage, swelling, and necrosis of mammalian liver cells [15].

To control the environmental risks of MCs, disinfection technology has been widely adopted to control MC-contaminated water and this exhibited obvious technical advantages [16,17]. MCs can be decomposed into low-toxicity or non-toxic substances by disinfectants that destroy the critical structures [18,19]. However, these processes might produce a variety of primary MC-related disinfection by-products (MC-DBPs) [19], which might retain the original toxic groups and thus produce potential inhibition effects on PPs [20,21].

A ligand–receptor interaction model could help extract the interaction parameters and explore the key interaction process. At present, information on the interactions between MC-DBPs and PPs is limited and interaction models for MC-DBP-PP complexes are not available. The relationship between the residual structure of MC-DBPs and biotoxicity is therefore not clear, and the mechanism for the potential inhibition effect of MC-DBPs on PPs is difficult to elucidate. The pioneering study of Xu et al. [22] provided a new viewpoint on evaluating the interactions between structural analogues and proteins without corresponding interaction models. They constructed interaction models for typical MC and PP2A complexes based on modeling ligand similarity and explored the important interactions based on molecular docking. The ligand-similarity approach not only helped to fill the gaps in the interaction models of MC structural analogs and proteins, but also explored the important interaction parameters, which was conducive to the study of the molecular mechanism.

In view of this, the modeling-based-on-ligand-similarity strategy and molecular docking simulation were adopted and integrated herein to explore the molecular mechanism of the potential inhibition effect of typical MCLR-DBPs on PP2As (the most important PPs in eukaryotic cells). Based on typical MCLR-DBPs derived from chlorine disinfection in the identification and preparation process, their inhibition effects on PP2A were evaluated by a traditional PPs inhibition assay [19]. With the assistance of molecular simulation, the interaction models for typical MCLR-DBPs and PP2A were constructed by modeling ligand similarity based on the crystal structure of the MCLR-PP2A complex. Subsequently, the candidate interaction parameters such as related areas, hydrogen bonds, metal bonds, and ionic bonds between the toxins and PP2A were obtained based on molecular docking simulation. By analyzing the correlation between inhibition data and candidate interaction parameters, the key interaction parameters were filtered. Further 2D ligand interaction analysis revealed the key sites and the key interactions between typical MCLR-DBPs and PP2A. Taking the key interactions into consideration, the molecular mechanism for the potential inhibition effect of typical MCLR-DBPs on PP2A was clarified in detail. Compared with the study of Xu et al. [22], our study considered that the disinfection process might affect the interactions between nine conserved amino acids of PP2A and Mn^{2+} ions/the introduced phosphate group, thus further explored the molecular mechanism for the potential inhibition effect of typical MCLR-DBPs on PP2A. Additionally, the analysis of the molecular mechanism was more comprehensive than that of Xu et al. [22]. We considered that the changed interactions affected by the disinfection process might be divided into multiple stages. Finally, the conditions and applications of the template docking mode were emphasized in the study herein. The current study draws increased attention to the secondary pollution caused by MC-DBPs. This study also contributes to development of an MCs regulation strategy, and therefore has important theoretical and practical application value.

2. Results and Discussions

2.1. Typical MCLR-DBPs Identification Based on MS and HPLC Analysis

Subject to chlorination, MCLR might convert into multiple typical MCLR-DBPs with different molecular weights that could be detected with a mass spectrometer (Figure 1). For MCLR ($C_{49}H_{74}N_{10}O_{12}$), its major MS signals could be detected at m/z 995.5559 and 996.5593 (the chief isotopic peak), corresponding to the singles of protonated toxin (Figure 1A). For the disinfection sample, five newly formed MS signals for single protonated typical MCLR-DBPs could be detected at m/z 1047.5276, 1029.5616, 1099.4991, 1081.5331, and 795.3995 (Figure 1B). With the assistance of Compass Isotope Pattern software, the chemical formulas for the above MCLR-DBPs could be identified as $C_{49}H_{75}N_{10}O_{13}Cl$ (+OH, +Cl), $C_{49}H_{76}N_{10}O_{14}$ (+2OH), $C_{49}H_{76}N_{10}O_{14}Cl_2$ (+2OH, +2Cl), $C_{49}H_{77}N_{10}O_{15}Cl$ (+3OH, +Cl), and $C_{34}H_{54}N_{10}O_{12}$ (−15C, −20H).

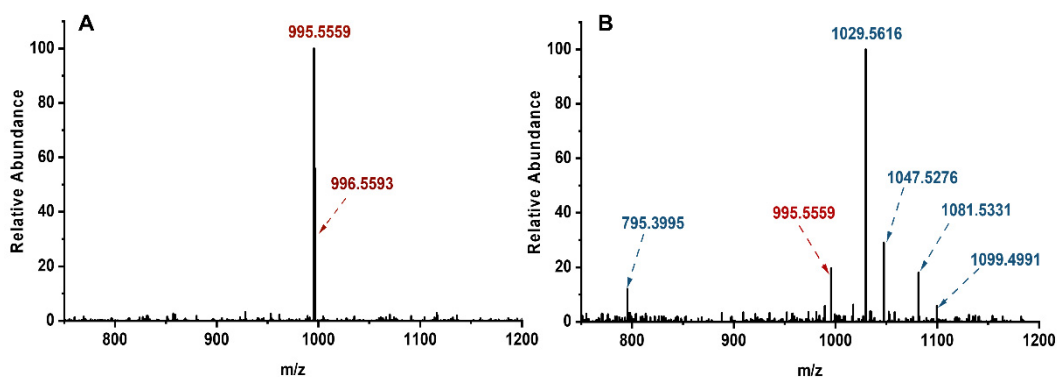


Figure 1. MS spectra for MCLR (A) and its disinfection sample (B) subject to chlorination for 40 min.

After solid-phase extraction, the preliminarily detected typical MCLR-DBPs in crude extract were purified by preparative chromatography separation. Simultaneously, the possible isomers for above MCLR-DBPs (with identical MS signals) could be separated and identified according to their extract ion chromatogram (EIC) peaks (Figure 2) and characteristic MS/MS fragments. For MCLR, it had a EIC peak around 18.25 min (Figure 2A) and several corresponding MS/MS fragments at m/z 213.0834, 286.1479, 553.3072, 599.3546, 682.3959, and 866.5150. With the assistance of Compass Isotope Pattern software, the typical MS/MS fragments could be identified as $[Glu^6-Mdha^7 + H]^+$, $[MeAsp^3-Arg^4 + H]^+$, $[Mdha^7-Ala^1-Leu^2-MeAsp^3-Arg^4 + H]^+$, $[MeAsp^3-Arg^4-Adda^5 + H]^+ / [Arg^4-Adda^5-Glu^6 + H]^+$, $[Arg^4-Adda^5-Glu^6-Mdha^7 + H]^+$, and $[Mdha^7-Ala^1-Leu^2-MeAsp^3-Arg^4-Adda^5 + H]^+ / [Arg^4-Adda^5-Glu^6-Mdha^7-Ala^1-Leu^2 + H]^+$ [20].

For typical MCLR-DBPs, eight EIC peaks were eluted between 16.82 min and 27.44 min (Figure 2A–F). By comparing the MS/MS fragments related to the newly formed EIC peaks with that of MCLR, it could be determined that Adda⁵ was the main reaction site (Table S1). Combined with chemical formula analysis, the generative mechanisms for the typical MCLR-DBPs were proposed: MCLR-DBP $C_{49}H_{75}N_{10}O_{13}Cl$ had two isomers that were eluted at 21.67 min (P1) and 22.29 min (P2) (Figure 2B). P1/P2 should be the addition products of 1·Cl + 1·OH to the conjugated diene of Adda⁵. According to Markovnikov's rule, Cl should be added to the C atom with more H atoms, while ·OH should be added to the C atom with less H atoms. On account of steric hindrance theory, the addition product to the inner double bond should have a lower abundance than the addition product to the external double bond. From this, P1 and P2 should be the addition product to the inner double bond and the addition product to the external double bond, respectively. For MCLR-DBP $C_{49}H_{76}N_{10}O_{14}$ with two EIC peaks at 17.44 min and 17.85 min (Figure 2C), it could be formed by the addition of 2·OH to the conjugated diene of Adda⁵ or transformed by substituting 1·Cl in the conjugated diene of P1/P2 with ·OH. Similarly, the addition product of the inner double bond (P3) should have a lower abundance than the external double bond (P4) on account of steric hindrance theory. For MCLR-DBP $C_{49}H_{76}N_{10}O_{14}Cl_2$ with

only one EIC peak at 27.44 min (Figure 2D), 2-Cl+2-OH should be successively added to the two double bonds and thus formed P5. Likewise, P5 also could be transformed from P1/P2 by adding 1-Cl + 1-OH to another C=C bond in Adda⁵. For MCLR-DBP C₄₉H₇₇N₁₀O₁₅Cl with two EIC peaks at 19.48 min and 20.09 min (Figure 2E), there should be two MCLR-DBP isomers P6/P7, which should be the secondary products of P1/P2/P3/P4. Taking the abundances of P1/P2/P3/P4 into account, P6 (the isomer with higher abundance) should be the secondary product of P1 and P4, while P7 (the isomer with lower abundance) should be the secondary product of P2 and P3. For MCLR-DBP C₃₄H₅₄N₁₀O₁₂ with only one EIC peak at 16.82 min (Figure 2F), the decreased molecular weight meant 15C+20H were removed from the side chain of Adda⁵ and 1C+1H+1O were left (P8). P8 could also be transformed from MCLR/P1/P3/P5/P6/P7 by the oxidation of inner double bonds, forming C=O bonds.

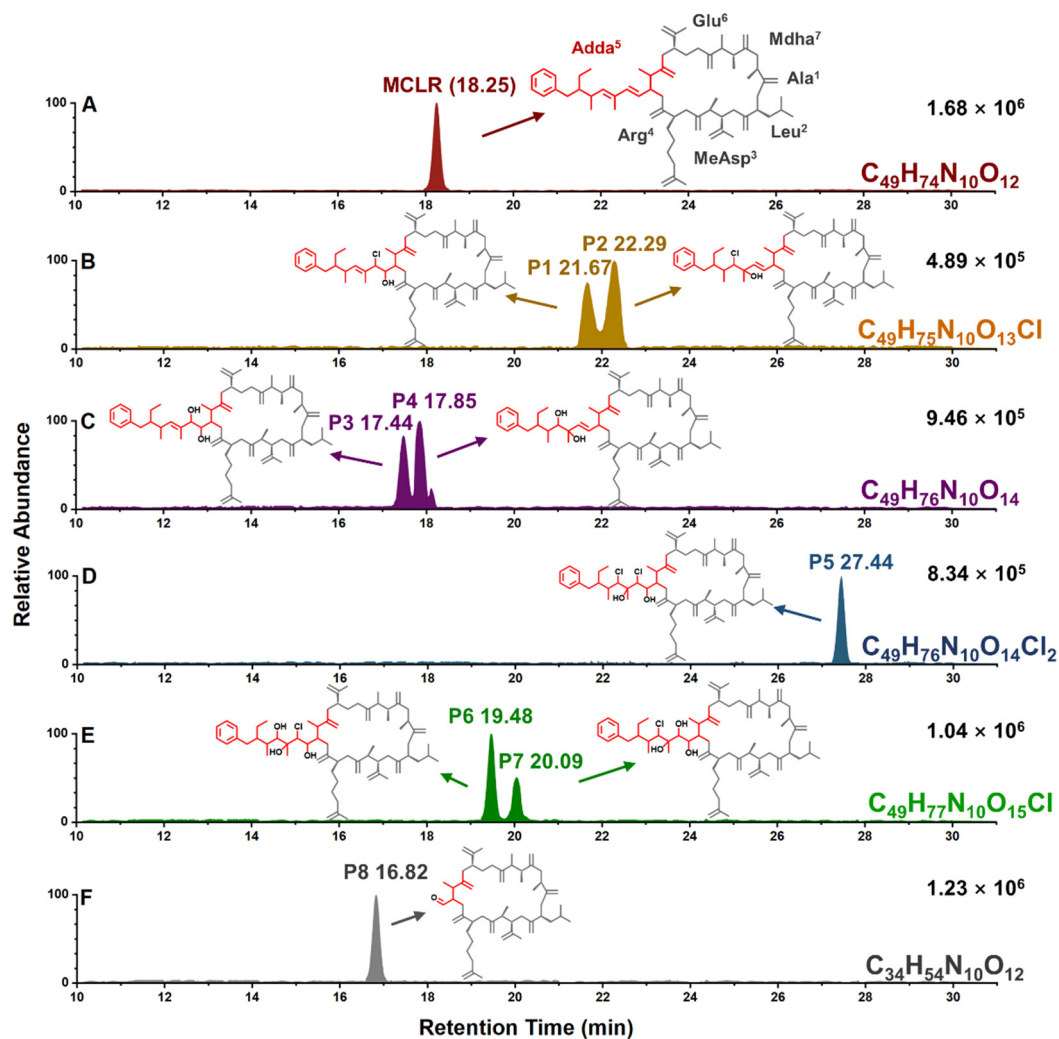


Figure 2. Extract ion chromatograms of native MCLR and typical MCLR-DBPs from disinfection sample (40 min, with their separate max. abundances fixed at 100%). Extract ion chromatograms of native MCLR (A), P1 and P2 (B), P3 and P4 (C), P5 (D), P6 and P7 (E), P8 (F).

2.2. Potential Inhibition Effect for Typical MCLR-DBPs Target to PP2A

Eluted typical MCLR-DBPs were collected around their specific retention times. The preparation and purification information for typical MCLR-DBPs was listed in Table S2. Due to their higher purity (>98.6%), the prepared MCLR-DBP samples were directly used in the PP2A inhibition assay. According to Figure 3, all of the typical MCLR-DBPs exhibited inhibition effects on PP2A. Compared with MCLR, the inhibition effect of typical MCLR-

DBPs decreased in different degrees. At 1 nM and 10 nM, the inhibition effect of toxins could be divided into six categories (a MCLR; b P1; c P4; d P2, P3; e P5, P6, P7; and f P8) according to ANOVA. At 100 nM, the inhibition effect of toxins could be divided into seven categories according to ANOVA: (a) MCLR; (ab) P1; (b) P4; (c) P3; (d) P2; (e) P7; (f) P6; and (g) P5, P8. To sum up, the inhibition sequence could be identified as MCLR > P1 > P4 > P3 ≈ P2 > P7 ≈ P6 ≈ P5 > P8. Basically, the inhibition effect of MCLR-DBPs on PP2A gradually decreased as the reaction progressed. What should be emphasized is the considerable inhibition effect of MCLR-DBPs (especially P1, P4) on PP2A; their secondary environmental risk could not be ignored.

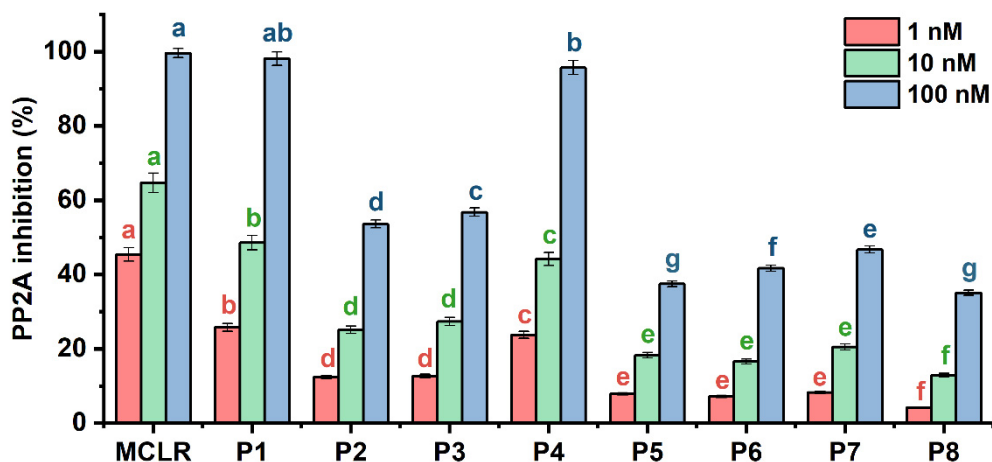


Figure 3. The inhibition effect of MCLR and typical MCLR-DBPs on PP2A. The error bar is the standard error of three repeated analyses. A one-way analysis of variance (ANOVA) followed by LSD post-hoc tests were used to verify significant differences among MCLR and MCLR-DBPs. Different letters indicate significant differences between groups ($p < 0.05$) obtained using SPSS software [23].

2.3. Simulation for the Interactions between Typical MCLR-DBPs and PP2A Based on Ligand Similarity Modeling and Molecular Docking

The potential inhibition effect of typical MCLR-DBPs on PP2A should be attributed to their residual toxic groups derived from MCLR. As limited information was available for the interactions between MCLR-DBPs and PP2A, it was difficult to evaluate the potential inhibition effect of typical MCLR-DBPs on PP2A. Since MCLR and MCLR-DBPs were considered to have a reasonable structural similarity, MCLR was an ideal template to construct MCLR-DBPs. With the assistance of molecular simulation, the models for typical MCLR-DBPs and PP2A were constructed by modeling based on ligand similarity (see Figure 4). The model for MCLR-PP2A was obtained from the Protein Data Bank (PDB code 2IE3) and preprocessed by “building missing loops” and adjusting the charges of the whole system. Based on the revised model for MCLR-PP2A, the models for typical MCLR-DBPs and PP2A complexes could be preliminarily constructed through “modeling based on ligand similarity”: the original ligand MCLR in the revised model was replaced by the identified MCLR-DBPs. Then, the models for MCLR-DBPs and PP2A complexes were energy minimized and re-docked through “template dock” mode to ensure the reliability of the models. On this basis, 80 candidate interaction parameters (combination areas, related surface areas, related chemical bonds) between toxins and PP2A, the exposure areas of the catalytic center, and related parameters for toxins were obtained with molecular docking simulation (listed in Table S3).

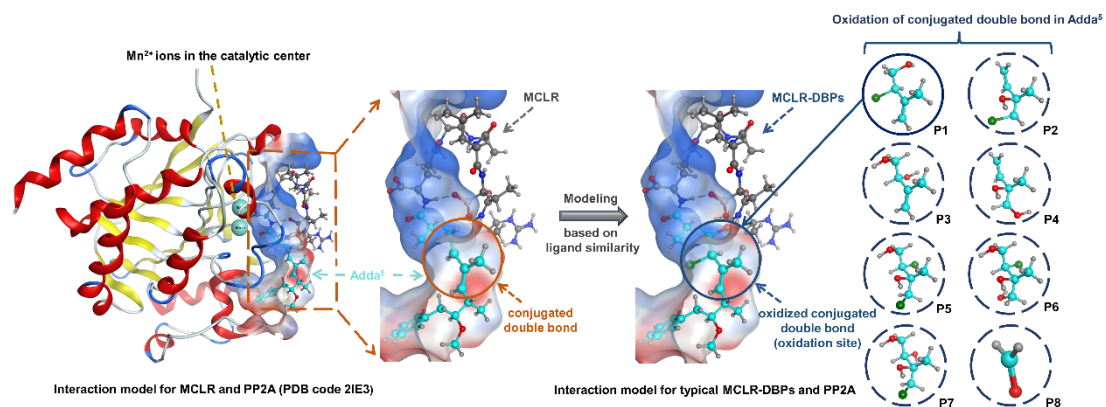


Figure 4. Illustration for interaction model construction for typical MCLR-DBP-PP2A complexes (with no PDB models) based on the ligand-similarity-modeling strategy.

2.4. Pearson Correlation Analysis for the Candidate Interaction Parameters and Inhibition Data

Pearson correlation analysis was used to evaluate the correlation between inhibition data and candidate interaction parameters. Regression analysis was not used to avoid deleting valid parameters associated with a few limited amino acid residues. According to Figures 5 and S1, the interaction parameters showed diversified correlation with inhibition data: 43 interaction parameters were positively correlated with inhibition data at all or partial concentrations, while 37 interaction parameters were negatively correlated with inhibition data at all or partial concentrations; 12 interaction parameters were extremely significantly correlated with inhibition data at all or partial concentrations ($p < 0.01$), while 24 interaction parameters were significantly correlated with inhibition data at all or partial concentrations ($p < 0.05$). Among them, the interaction parameters that were significantly or extremely significantly correlated with inhibition data ($p < 0.05$ or $p < 0.01$) were crucial for the inhibition effect of MCLR and typical MCLR-DBPs on PP2A.

In view of this, Venn diagrams were further used to screen the key interaction parameters (Figure 6). At the level of $p < 0.01$, the catalytic center exposure area for Asp⁵⁷ + Mn²⁺, hydrogen bonds for Arg⁴←Arg²¹⁴, “Adda⁵”←His¹¹⁸, and the combination area for MeAsp³→PP2A were highly and significantly correlated with toxin toxicity at the three test concentrations. Hydrogen bond for Arg⁴→Pro²¹³, ionic bond for Glu⁶-Arg⁸⁹, the combination areas for Ala¹→PP2A, Glu⁶→PP2A, the negative accessible surface area for Ala¹→PP2A, the positive accessible surface area for Glu⁶→PP2A, and the amino acid associated with the binding of the phosphate group for Arg²¹⁴ were highly and significantly correlated with toxin toxicity at 1 nM and 10 nM. The combination area for “Adda⁵”→PP2A was highly and significantly correlated with toxin toxicity at 10 nM and 100 nM. At the level of $p < 0.05$, the combination area for Arg⁴→PP2A, the positive accessible surface area for “Adda⁵”→PP2A, the hydrophobic surface area for “Adda⁵”→PP2A, and the polar surface area for “Adda⁵”→PP2A were in highly significant correlation with toxin toxicity at the three test concentrations. The metal bonds for Mn²⁺ ions to toxins, the metal bond for Glu⁶-Mn²⁺, and the polar surface area for Leu²→PP2A were significantly correlated with toxin toxicity at 1 nM and 10 nM. Hydrogen bonds for MeAsp³←Arg⁸⁹, “Adda⁵”←Asn¹¹⁷, ionic bonds for Arg⁸⁵-Mn²⁺, Arg⁵⁷-Mn²⁺, metal bond for Glu⁶-Mn²⁺, and the combination area for Mdha⁷→PP2A were significantly correlated with toxin toxicity at 10 nM and 100 nM. The combination area for “Adda⁵”→PP2A, the polar surface area for MeAsp³→PP2A, and the hydrophobic surface area for Arg⁴→PP2A were significantly correlated with toxin toxicity at 1 nM. The positive accessible surface area for Ala¹→PP2A and the hydrophobic surface area for Leu²→PP2A were significantly correlated with toxin toxicity at 10 nM. Hydrogen bond for Arg⁴→Pro²¹³, ionic bond for Glu⁶-Arg⁸⁹, the combination areas for Ala¹→PP2A, Glu⁶→PP2A, the negative accessible surface area for Ala¹→PP2A, and the positive accessible surface area for Glu⁶→PP2A were significantly correlated with toxin toxicity at 100 nM. Obviously, the above interaction parameters (especially those

highly related to toxin toxicity at two and three test concentrations) were important for the inhibition effect of MCLR and typical MCLR-DBPs on PP2A.

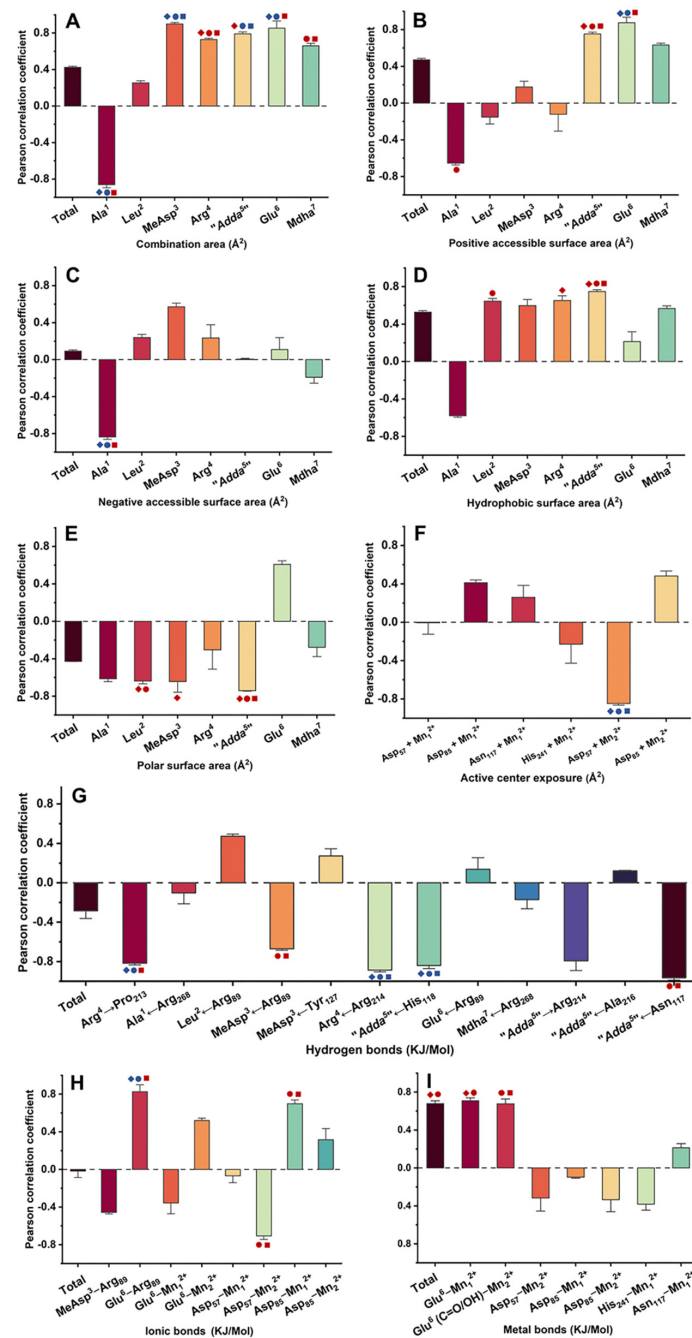


Figure 5. Pearson correlation coefficient between inhibition data and (A) combination area, (B) positive accessible surface area, (C) negative accessible surface area, (D) hydrophobic surface area, (E) polar surface area, (F) active center exposure, (G) hydrogen bonds, (H) ionic bonds, (I) metal bonds. Conditions: the interaction parameters that were significantly or highly significantly correlated with inhibition data ($p < 0.05$ or $p < 0.01$) are marked with symbols in different colors. The interaction parameters that had significantly or highly significantly correlations correlated with inhibition data at different toxin levels are marked with symbols in different shapes. \blacklozenge , \bullet , \blacksquare mean that the interaction parameters are extremely and significantly correlated with the inhibition data at the levels of 1, 10, and 100 nM, respectively ($p < 0.01$). \blacklozenge , \bullet , \blacksquare mean that the interaction parameters are significantly correlated with the inhibition data at the levels of 1, 10, and 100 nM, respectively ($p < 0.05$). A Student's *t*-test was applied to the Pearson correlation analysis.

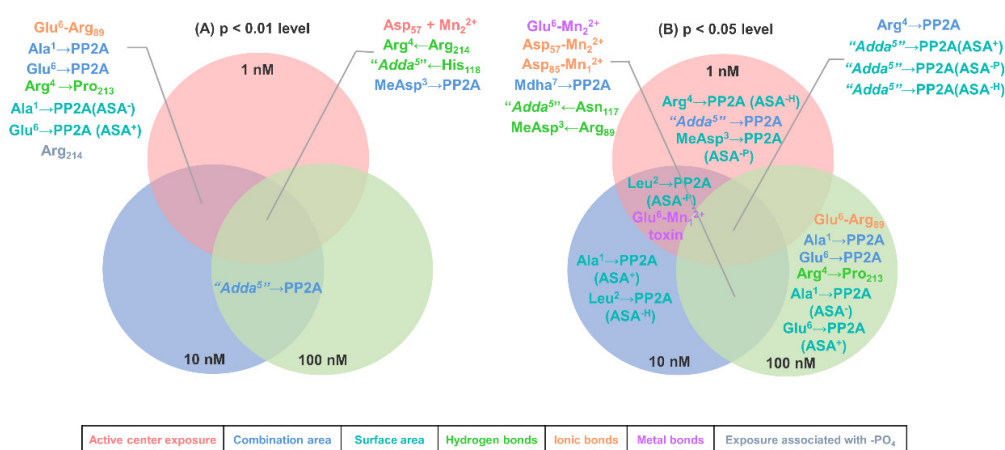


Figure 6. Venn diagrams of the significant interaction parameters at the $p < 0.01$ level (A) and $p < 0.05$ level (B). Conditions: ASA⁺ stands for positive accessible surface area, ASA⁻ stands for negative accessible surface area, ASA^H stands for hydrophobic surface area, and ASA^P stands for polar surface area.

The statistical analysis was further adopted to classify the key interactions based on the structural units of MCLR/MCLR-DBPs and catalytic center (Figure 7). Among this, the metal bonds for Mn²⁺ ions to toxins should be related to Glu⁶, Mn₁²⁺ ion, and Mn₂²⁺ ion. Statistical frequency analysis (Figure 7A) determined that six key interaction parameters were related to "Adda⁵" / Glu⁶, four key interaction parameters were related to Arg⁴ / Mn₂²⁺, three key interaction parameters were related to Ala¹ / MeAsp³ / Mn₁²⁺, two key interaction parameters were related to Leu², while one key interaction parameter was related to the phosphate group / Mdha⁷. Combined with statistical analysis for the total $|\bar{R}|$ values related to the above sites, "Adda⁵", Glu⁶, Arg⁴, Mn₂²⁺ ion, Ala¹, MeAsp³, Mn₁²⁺ ion, Leu², the phosphate group, and Mdha⁷ participated in the combination of MCLR/MCLR-DBPs to PP2A and their contributions exhibited a downward trend. "Adda⁵" / Glu⁶ had a prominent influence on the combination of MCLR/MCLR-DBPs to PP2A, Arg⁴ / Mn₂²⁺ / Ala¹ / MeAsp³ / Mn₁²⁺ had a considerable influence on the combination of MCLR/MCLR-DBPs to PP2A, while Leu² / the phosphate group / Mdha⁷ had certain influence on the combination of MCLR/MCLR-DBPs to PP2A (Figure 7B).

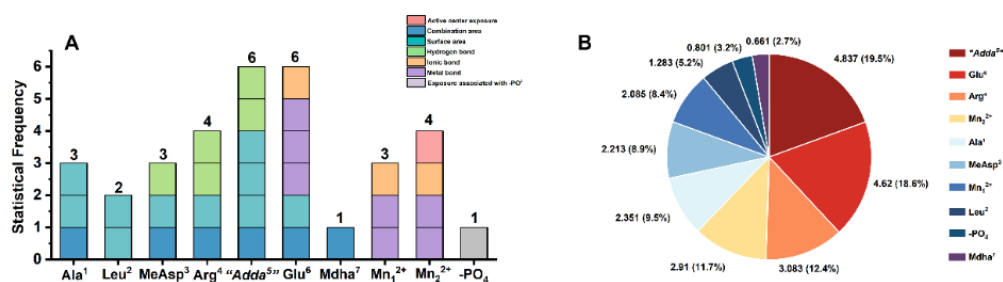


Figure 7. Histogram for the statistical frequency (A) related to the key interaction sites and pie chart for the total $|\bar{R}|$ values (B) related to the key interaction sites. Conditions: \bar{R} is the average of Pearson correlations at three toxin concentrations.

2.5. Molecular Mechanism Analysis for the Potential Inhibition Effect of Typical MCLR-DBPs Target to PP2A

The 2D ligand–receptor interaction diagram illustrated the key interactions, including hydrogen bonds "Adda⁵" ← Asn₁₁₇, "Adda⁵" ← His₁₁₈, Arg⁴ ← Arg₂₁₄, Arg⁴ → Pro₂₁₃, MeAsp³ ← Arg₈₉; ionic bonds Glu⁶-Arg₈₉, Asp₈₅-Mn₁²⁺, Asp₅₇-Mn₂²⁺; and metal bonds Glu⁶-Mn₁²⁺, Glu⁶-Mn₂²⁺ (Figure 8). The identified MCLR-DBPs retained all or part of the key sites (key interactions), and thus exhibited potential inhibition effects on PP2A. With

the progress of the chlorination, the structure of Adda⁵ was gradually destroyed and the inhibition effect of typical MCLR-DBPs on PP2A basically decreased as well. Obviously, structural differences changed the above key interactions and thus changed the inhibition effects of typical MCLR-DBPs on PP2A.

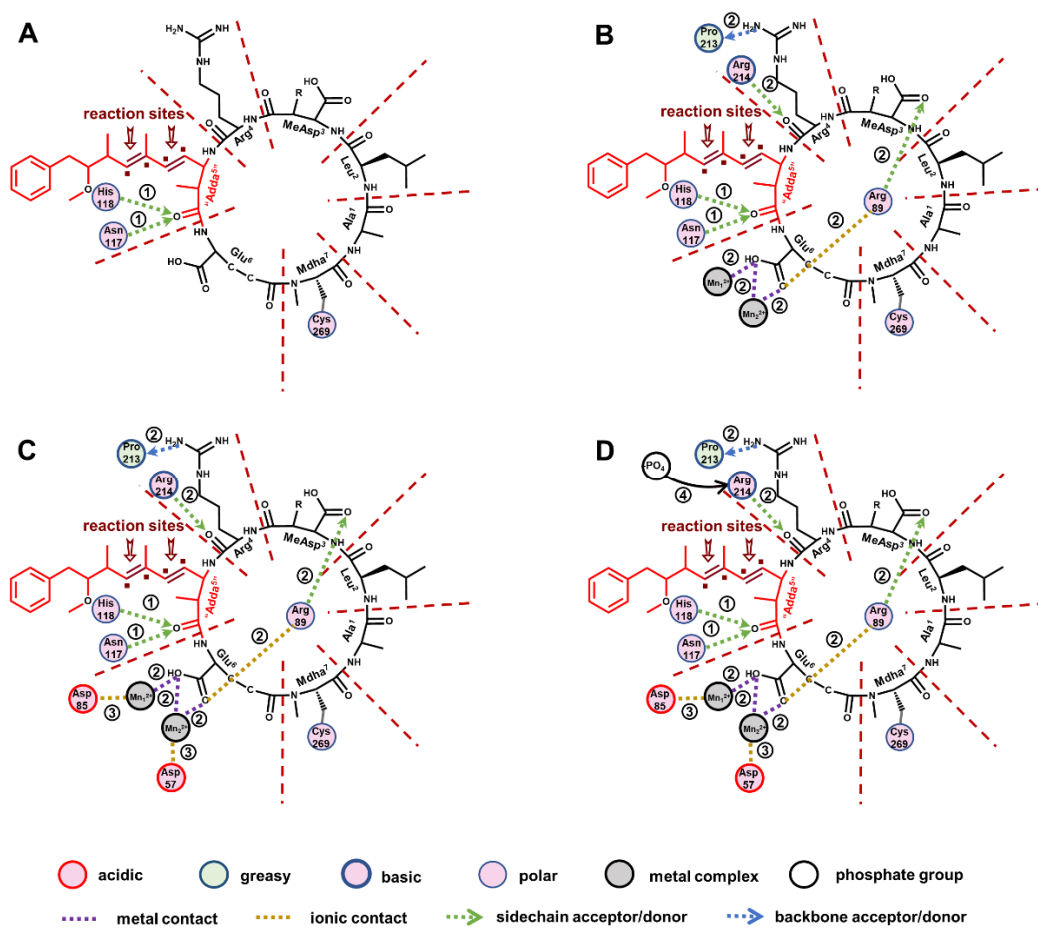


Figure 8. The 2D ligand–receptor interaction diagram for the combination of the toxins to PP2A. The direct influence of damaged “Adda⁵” on the interactions between toxins and PP2A (A). The indirect influence of damaged “Adda⁵” on the interactions between toxins and PP2A (B). The influence of the changed interactions on the interactions involving Mn²⁺ ions (C). The influence of the changed interaction on the exposure of amino acids bound to phosphate group (D).

More specifically, the introduced polar groups ·Cl and ·OH firstly weakened the hydrophobic and electropositive interactions between “Adda⁵” and PP2A (ASA^{-H} and ASA⁺ related to “Adda⁵” were positively correlated with toxicity), resulting in the attenuated combination of “Adda⁵” to PP2A. The progressive damage of “Adda⁵” directly weakened hydrogen bonds “Adda⁵”←Asn₁₁₇ and “Adda⁵”←His₁₁₈ to larger degrees. The progressive damage of “Adda⁵” also intervened in the combination of other structural units of MCLR-DBPs to PP2A by weakening hydrogen bonds MeAsp³←Arg₈₉, Arg⁴←Arg₂₁₄, Arg⁴→Pro₂₁₃, and by strengthening ionic bond Glu⁶-Arg₈₉. Correspondingly, the combination areas of MeAsp³ and Arg⁴ to PP2A were decreased. However, the combination areas of Glu⁶ to PP2A did not show an increase trend. The abnormal phenomenon should be attributed to the competitive effect of Mn²⁺ ions in the catalytic center. The two Mn²⁺ ions could form new metal bonds (Glu⁶-Mn²⁺, Glu⁶(C=O)-Mn²⁺, Glu⁶(OH)-Mn²⁺) with the side chain of Glu⁶. The above modified interactions further affected the interactions between the conserved domain of PP2A and Mn²⁺ ions (including the enhanced ionic bond Asp₈₅-Mn²⁺ and the weakened ionic bond Asp₅₇-Mn²⁺) and promoted the exposure of

Mn²⁺ ions. At the same time, weakening of the hydrogen bond Arg⁴←Arg₂₁₄ promoted the exposure areas of Arg₂₁₄, and thus the linkage of the phosphate group to Arg₂₁₄ was facilitated. Both the exposure of Mn²⁺ ions and the combination of Arg₂₁₄ to the phosphate group increased, resulting in the restored catalytic activity of PP2A.

3. Conclusions

This research investigated the molecular mechanism for the potential inhibition effect of typical MCLR-DBPs target to PP2A. Subject to disinfection, MCLR was oxidized into five types of typical MCLR-DBP with different molecular weights. The isomers for typical MCLR-DBPs with identical molecular weight were separated and identified as P1–P8 (mainly the ·OH/·Cl addition products related to the conjugated diene in Adda⁵). PP2A inhibition assay showed that the potential inhibition effects of toxins were in the sequence of MCLR > P1 > P4 > P3 ≈ P2 > P7 ≈ P6 ≈ P5 > P8. To elucidate the molecular mechanism underlying the inhibition effect, the interaction models for typical MCLR-DBPs-PP2A were preliminary constructed by a modeling-based-on-ligand-similarity strategy according to the crystal structure of the MCLR-PP2A complex. With the assistance of molecular docking simulation, the candidate interaction parameters between typical MCLR-DBPs and PP2A were obtained. Taking the inhibition data and candidate interaction parameters into consideration, Pearson correlation analysis filtered the key interaction parameters. The progressive damage of “Adda⁵” directly resulted in the weakening of hydrogen bonds “Adda⁵←Asn₁₁₇ and “Adda⁵←His₁₁₈, and indirectly resulted in the weakening of hydrogen bonds MeAsp³←Arg₈₉, Arg⁴←Arg₂₁₄, Arg⁴→Pro₂₁₃, and the strengthening of ionic bond Glu⁶-Arg₈₉. Changes in the above key interactions further affected the interactions associated with Mn²⁺ ions (in the catalytic center) by strengthening ionic bond Asp₈₅-Mn₁²⁺, metal bonds Glu⁶-Mn₁²⁺, Glu⁶-Mn₂²⁺, and weakening ionic bond Asp₅₇-Mn₂²⁺. The typical MCLR-DBPs retained the above key interactions, and thus exhibited potential inhibition effects on PP2A. Changes in the interactions associated with Mn²⁺ ions increased the exposure areas of Mn²⁺ ions. Meanwhile, the weakened hydrogen bond Arg⁴←Arg₂₁₄ facilitated the linkage of the phosphate group to Arg₂₁₄ (with increased exposure). In this way, the catalytic activity of PP2A was restored.

4. Materials and Methods

4.1. Materials

Microcystin-LR was purchased from Sigma (Saint-Quentin Fallavier, France). PP2A was obtained from New England Biolabs Inc. Na₂S₂O₃, MgCl₂, MnCl₂, HCl, Ca(ClO)₂, high-purity CO₂, p-Nitrophenyldisodium orthophosphate (p-NPP), tris(hydroxymethyl) aminomethane (Tris), bovine serum albumin (BSA), dithiothreitol (DTT), neoprene rubber, sodium nitrobenzene disodium, and ascorbic acid were purchased from Sinopharm (Shanghai, China). HCOOH, CH₃OH, CF₃COOH, and HPLC acetonitrile were purchased from Merck (Darmstadt, Germany).

4.2. Chlorination Treatment of MCLR

Chlorination treatment of MCLR was performed with HClO serving as the disinfectant. HClO was prepared based on the precipitation reaction of Ca(ClO)₂ and CO₂ [24]. Amounts of 250 mL MCLR (100 µg/L) and 250 mL HClO (about 4 mg/L) were mixed in a 1000 mL brown reagent bottle and reacted in darkness at room temperature. At the fixed reaction time, 50 mL disinfection sample was fetched out and mixed with 5 mL ascorbic acid (about 20 mg/L).

4.3. Purification and Preparation of Typical MCLR-DBPs

4.3.1. MS Analysis of the Disinfection Samples

The chlorination sample was mixed with the same volume of methanol (containing 0.1% formic acid) and was injected into a maXis UHR-TOF mass spectrometer for the preliminary identification of typical MCLR-DBPs. Typical MS parameters were set as

follows: positive ion spray ionization pattern, source voltage 4 kV, cone voltage 0.5 kV, desolvation gas (N₂) 0.4 bar, dry gas (N₂) heater 180 °C, dry gas (N₂) flow rate 4 L/min, full scan m/z 750–1200.

4.3.2. Purification of Typical MCLR-DBPs

According to the traditional concentration and enrichment methods for MCs, typical MCLR-DBPs were purified [25,26]. Disinfection samples (50 mL) were applied to the pre-rinsed SepPakC₁₈ SPE cartridges (1000 mg, Waters) with 10 mL methanol and 10 mL high purity water. Impurities and typical MCLR-DBPs were eluted with 5 mL 10% methanol and 5 mL 80% methanol, respectively. The crude extracts of typical MCLR-DBPs were evaporated to dryness in N₂ flow and resuspended in 200 µL 20% acetonitrile. Then the crude extracts were separated using a Dionex Ultimate-3000 HPLC system equipped with a C₁₈ reversed-phase preparative column (25.4 mm × 450 mm, 5 µm, 120 Å) [21]. Water (containing 0.1% formic acid) and acetonitrile (containing 0.1% formic acid) were used as mobile phase A and mobile phase B, respectively. The elution conditions were: 20% mobile phase B for 3 min; 20%→80% mobile phase B over 25 min; 80%→20% mobile phase B within 0.1 min; 20% mobile phase B for 3 min. The column temperature and the flow rate were set at 35 °C and 5 mL/min, respectively.

4.3.3. Preparation of Typical MCLR-DBPs

At the same time, partial chromatographic effluent was guided into the maXis UHR-TOF mass spectrometer through a four-way valve with the assistance of an autosampler. MS parameters were set as those of Section 4.3.1 except “full scan” mode was changed to “selective ion scan” mode. The specific retention times for typical MCLR-DBPs (especially for the isomers) could be obtained. Chromatography-separated typical MCLR-DBPs were collected at their specific retention times and separately stored in brown reagent bottles [21]. Multi-collect pure samples for typical MCLR-DBPs were dried with N₂ and dissolved in 200 µL methanol. Based on MS/MS analysis, the prepared MCLR-DBPs were identified by comparing their secondary structures with that of MCLR (MS/MS parameters were set as those of Section 4.3.1 except N₂ collision gas energies were adjusted from 40 to 100 eV, and full scan range was adjusted as m/z 100–1200).

4.4. PP2A Inhibition Assay for MCLR and Typical MCLR-DBPs

The inhibition effect of typical MCLR-DBPs on PP2A was evaluated with a typical protein phosphatase inhibition assay [27]. First, PP2A was diluted to 5 U/mL with buffer solution (50 mM Tris-HCl, 1.0 mM MnCl₂, 2.0 mM dithiothreitol, pH 7.4) and 1.0 g/L BSA. Afterwards, 10 µL PP2A and 100 µL samples were mixed into a 96-well polystyrene microplate plate. After shaking slightly, the microplate was kept at 25.0 °C for 15 min and 90 µL p-NPP was added to the microtiter plate. After 60 min, absorbance ODS₄₀₅ was measured with a microplate reader. The PP2A relative activity percentage formula is as follows: $I_{PP2A} (\%) = (A_{toxins} - A_{blank}) / (A_{control} - A_{blank}) \times 100\%$. In the control group, toxins were replaced by distilled water, and in the blank group MCLR/MCLR-DBPs and PP2A were replaced by distilled water.

4.5. Molecular Simulation for the Interactions between MCLR/MCLR-DBPs and PP2A

Molecular simulation was performed with Molecular Operating Environment software (MOE, version 20.09). The experimental steps were as follows: The model for MCLR-PP2A was obtained from Protein Data Bank (PDB code 2IE3). When the model for the MCLR-PP2A complex was introduced into MOE, MCLR and PP2A were preprocessed by “building missing loops” and adjusting the charges of the whole system [28]. The models for MCLR-DBPs-PP2A were preliminarily constructed by modeling based on ligand similarity: the original ligand MCLR in the optimized model of MCLR-PP2A was replaced by different MCLR-DBPs [22,28]. The models for MCLR-DBPs-PP2A complexes were energy-minimized to determine the optimal interaction geometry and associated

energy between MCLR-DBPs and PP2A and to check the rationality of crystal structures. Subsequently, the optimized models for MCLR-DBPs-PP2A complexes were re-docked through “template dock” mode and then the interactions between MCLR/MCLR-DBPs and PP2A were simulated. The “template dock” mode developed by MOE software was suitable for binding sites whose locations are known but information about specific ligand interactions is lacking, which ensured the comparability of MCLR-DBPs with their original toxin [22]. Docking parameters were set as follows: amber 10 EHT, solvation r-field, temperature 25.0 °C, pH 7.4, salinity 0.05 M. The candidate interaction parameters (combination areas, related surface areas, hydrogen bonds, metal bonds, ionic bonds, exposure areas of the catalytic center) related to the combination of toxins to PP2A could be obtained.

4.6. Statistical Analysis

Pearson correlation analysis was used to analyze the correlations between inhibition data and candidate interaction parameters with IBM SPSS Statistics software (version 26.0, Chicago, IL, USA). Hypothesis testing of Pearson correlation coefficient was performed with Student’s *t*-test. Significance levels are reported to be highly significant ($p < 0.01$), significant ($p < 0.05$), or not significant ($p > 0.05$). One-way analysis of variance (ANOVA) followed by least significant difference (LSD) post-hoc tests was used to check significant differences among groups and $p < 0.05$ values were considered statistically significant.

Supplementary Materials: The following supporting information can be downloaded at: <https://www.mdpi.com/article/10.3390/toxins14120878/s1>, Table S1: MS/MS identification of MCLR and MCLR-DBPs; Table S2: Preparation and purification information for typical MCLR-DBPs; Table S3: The candidate interaction parameters between MCLR/MCLR-DBPs and PP2A; Figure S1: Pearson correlation coefficients between inhibition data and exposure areas associated with phosphate group.

Author Contributions: Conceptualization, W.Z. and H.Y.; methodology, W.Z. and H.Y.; writing—original draft preparation, H.Y.; writing—review and editing, W.Z. and H.Y.; supervision, Y.X. and J.C. All authors have read and agreed to the published version of the manuscript.

Funding: This work is supported by the National Natural Science Foundation of China (21876103).

Institutional Review Board Statement: Not applicable.

Informed Consent Statement: Not applicable.

Data Availability Statement: Not applicable.

Conflicts of Interest: The authors declare no conflict of interest.

References

1. Wilhelm, S.W.; Bullerjahn, G.S.; McKay, R.M.L. The Complicated and Confusing Ecology of Microcystis Blooms. *Mbio* **2020**, *11*, 3. [CrossRef] [PubMed]
2. Guo, Y.; O’Brien, A.M.; Lins, T.F.; Shahmohamadloo, R.S.; Almirall, X.O.; Rochman, C.M.; Sinton, D. Effects of Hydrogen Peroxide on Cyanobacterium *Microcystis aeruginosa* in the Presence of Nanoplastics. *ACS ES T Water* **2021**, *1*, 1596–1607. [CrossRef]
3. Ortea, P.M.; Allis, O.; Healy, B.M.; Lehane, M.; Ni Shuilleabhain, A.; Furey, A.; James, K.J. Determination of toxic cyclic heptapeptides by liquid chromatography with detection using ultra-violet, protein phosphatase assay and tandem mass spectrometry. *Chemosphere* **2004**, *55*, 1395–1402. [CrossRef] [PubMed]
4. Chen, L.; Chen, J.; Zhang, X.; Xie, P. A review of reproductive toxicity of microcystins. *J. Hazard. Mater.* **2016**, *301*, 381–399. [CrossRef] [PubMed]
5. Kordasht, H.K.; Hassanpour, S.; Baradaran, B.; Nosrati, R.; Hashemzaei, M.; Mokhtarzadeh, A.; la Guardia, M. Biosensing of microcystins in water samples; recent advances. *Biosens. Bioelectron.* **2020**, *165*, 112403. [CrossRef]
6. Welten, R.D.; Meneely, J.P.; Elliott, C.T. A Comparative Review of the Effect of Microcystin-LR on the Proteome. *Expo. Health* **2019**, *12*, 111–129. [CrossRef]
7. Du, B.B.; Liu, G.F.; Ke, M.J.; Zhang, Z.Y.; Zheng, M.; Lu, T.; Sun, L.W.; Qian, H.F. Proteomic analysis of the hepatotoxicity of *Microcystis aeruginosa* in adult zebrafish (*Danio rerio*) and its potential mechanisms. *Environ. Pollut.* **2019**, *254*, 113019. [CrossRef]
8. Svircev, Z.; Drobac, D.; Tokodi, N.; Mijovic, B.; Codd, G.A.; Meriluoto, J. Toxicology of microcystins with reference to cases of human intoxications and epidemiological investigations of exposures to cyanobacteria and cyanotoxins. *Arch. Toxicol.* **2017**, *91*, 621–650. [CrossRef]

9. Gullede, B.M.; Aggen, J.B.; Eng, H.; Sweimeh, K.; Chamberlin, A.R. Microcystin analogues comprised only of Adda and a single additional amino acid retain moderate activity as PP1/PP2A inhibitors. *Bioorg. Med. Chem. Lett.* **2003**, *13*, 2907–2911. [[CrossRef](#)]
10. Craig, M.; Luu, H.A.; McCready, T.L.; Holmes, C.F.B.; Williams, D.; Andersen, R.J. Molecular mechanisms underlying the interaction of motuporin and microcystins with type-1 and type-2A protein phosphatases. *Biochem. Cell Biol.* **1996**, *74*, 569–578. [[CrossRef](#)]
11. Fontanillo, M.; Kohn, M. Microcystins: Synthesis and structure-activity relationship studies toward PP1 and PP2A. *Bioorg. Med. Chem.* **2018**, *26*, 1118–1126. [[CrossRef](#)] [[PubMed](#)]
12. Zhang, Q.; Fan, Z.; Zhang, L.; You, Q.; Wang, L. Strategies for Targeting Serine/Threonine Protein Phosphatases with Small Molecules in Cancer. *J. Med. Chem.* **2021**, *64*, 8916–8938. [[CrossRef](#)] [[PubMed](#)]
13. Campos, A.; Vasconcelos, V. Molecular mechanisms of microcystin toxicity in animal cells. *Int. J. Mol. Sci.* **2010**, *11*, 268–287. [[CrossRef](#)] [[PubMed](#)]
14. Nishiwaki-Matsushima, R.; Ohta, T.; Nishiwaki, S.; Suganuma, M.; Kohyama, K.; Ishikawa, T.; Carmichael, W.W.; Fujiki, H. Liver tumor promotion by the cyanobacterial cyclic peptide toxin microcystin-LR. *J. Cancer Res. Clin. Oncol.* **1992**, *118*, 420–424. [[CrossRef](#)] [[PubMed](#)]
15. Beasley, V.R.; Cook, W.O.; Dahlem, A.M.; Hooser, S.B.; Lovell, R.A.; Valentine, W.M. Algae intoxication in livestock and waterfowl. *Vet. Clin. N. Am. Food Anim. Pract.* **1989**, *5*, 345–361. [[CrossRef](#)] [[PubMed](#)]
16. Tsuji, K.; Watanuki, T.; Kondo, F.; Watanabe, M.F.; Nakazawa, H.; Suzuki, M.; Uchida, H.; Harada, K. Stability of microcystins from cyanobacteria—IV. Effect of chlorination on decomposition. *Toxicon Off. J. Int. Soc. Toxinol.* **1997**, *35*, 1033–1041. [[CrossRef](#)]
17. Duan, X.; Sanan, T.; de la Cruz, A.; He, X.; Kong, M.; Dionysiou, D.D. Susceptibility of the Algal Toxin Microcystin-LR to UV/Chlorine Process: Comparison with Chlorination. *Environ. Sci. Technol.* **2018**, *52*, 8252–8262. [[CrossRef](#)]
18. Hu, Z.; Wang, X.; Zhang, S.; Zong, W. Research on the discrepant inhibition mechanism of microcystin-LR disinfectant by-products target to protein phosphatase 1. *Environ. Sci. Pollut. Res. Int.* **2021**, *28*, 45586–45595. [[CrossRef](#)]
19. Zong, W.; Sun, F.; Sun, X. Evaluation on the generative mechanism and biological toxicity of microcystin-LR disinfection by-products formed by chlorination. *J. Hazard. Mater.* **2013**, *252–253*, 293–299. [[CrossRef](#)]
20. Zong, W.; Sun, F.; Pei, H.; Hu, W.; Pei, R. Microcystin-associated disinfection by-products: The real and non-negligible risk to drinking water subject to chlorination. *Chem. Eng. J.* **2015**, *279*, 498–506. [[CrossRef](#)]
21. Zong, W.; Sun, F.; Sun, X. Oxidation by-products formation of microcystin-LR exposed to UV/H₂O₂: Toward the generative mechanism and biological toxicity. *Water Res.* **2013**, *47*, 3211–3219. [[CrossRef](#)] [[PubMed](#)]
22. Xu, Y.; Cui, J.; Yu, H.; Zong, W. Insight into the Molecular Mechanism for the Discrepant Inhibition of Microcystins (MCLR, LA, LF, LW, LY) on Protein Phosphatase 2A. *Toxins* **2022**, *14*, 390. [[CrossRef](#)] [[PubMed](#)]
23. Park, E.; Cho, M.; Ki, C.S. Correct Use of Repeated Measures Analysis of Variance. *Korean J. Lab. Med.* **2009**, *29*, 1–9. [[CrossRef](#)] [[PubMed](#)]
24. Yigit, O.; Soyuncu, S.; Eray, O.; Enver, S. Inhalational and dermal injury due to explosion of calcium hypochlorite. *Cutan. Ocul. Toxicol.* **2009**, *28*, 37–40. [[CrossRef](#)] [[PubMed](#)]
25. An, J.; Carmichael, W.W. Use of a colorimetric protein phosphatase inhibition assay and enzyme linked immunosorbent assay for the study of microcystins and nodularins. *Toxicon Off. J. Int. Soc. Toxinol.* **1994**, *32*, 1495–1507. [[CrossRef](#)] [[PubMed](#)]
26. Sun, F.; Pei, H.-Y.; Hu, W.-R.; Song, M.-M. A multi-technique approach for the quantification of *Microcystis aeruginosa* FACHB-905 biomass during high algae-laden periods. *Environ. Technol.* **2012**, *33*, 1773–1779. [[CrossRef](#)]
27. Ward, C.J.; Beattie, K.A.; Lee, E.Y.; Codd, G.A. Colorimetric protein phosphatase inhibition assay of laboratory strains and natural blooms of cyanobacteria: Comparisons with high-performance liquid chromatographic analysis for microcystins. *FEMS Microbiol. Lett.* **1997**, *153*, 465–473. [[CrossRef](#)]
28. Chen, H.; Fu, W.; Wang, Z.; Wang, X.; Lei, T.; Zhu, F.; Li, D.; Chang, S.; Xu, L.; Hou, T. Reliability of Docking-Based Virtual Screening for GPCR Ligands with Homology Modeled Structures: A Case Study of the Angiotensin II Type I Receptor. *ACS Chem. Neurosci.* **2019**, *10*, 677–689. [[CrossRef](#)]